



PR12-25-010, JLab PAC 53

Double Deeply Virtual Compton Scattering with SoLID μ spectrometer

Juan-Sebastian Alvarado, IJCLab
Alexandre Camsonne, Jlab (contact)

Marie Boer, Virginia Tech

Eric Voutier, IJCLab

Xinzhan Bai, JLab

Zhiwen Zhao, Duke (presenter)

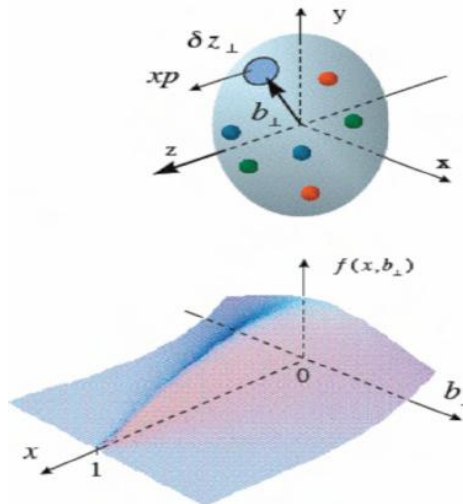
and SoLID Collaboration

July 21, 2025

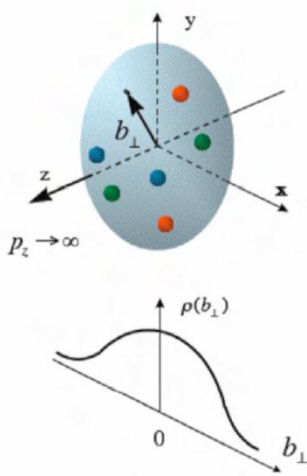
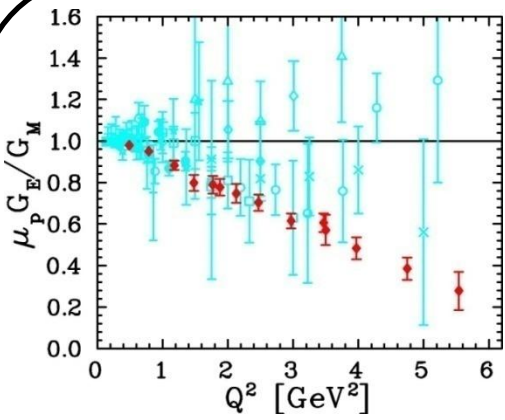
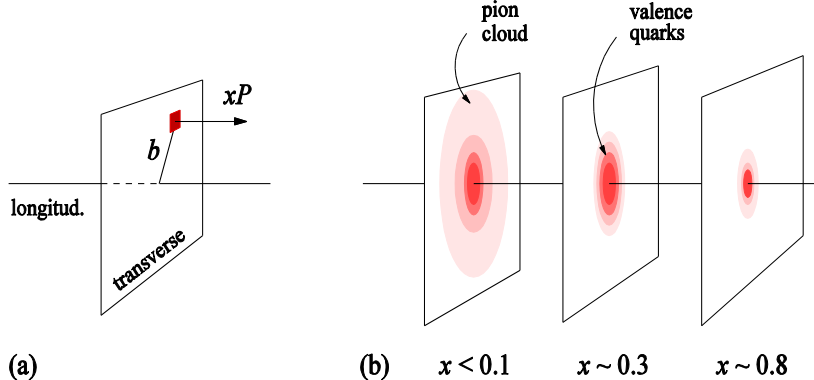
Outline

- Generalized Parton Distribution
- Double Deeply Virtual Compton Scattering
- SoLID μ setup
- Muon detector
- Simulation study
- Physics projection
- Beam time request
- Summary

Generalized Parton Distribution (GPD)

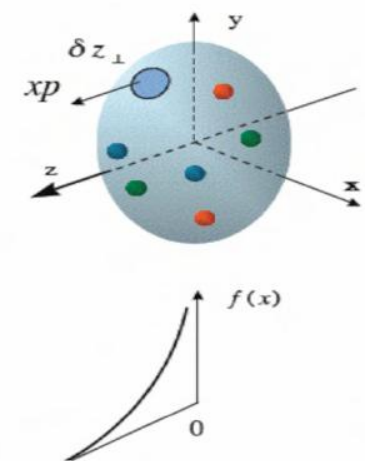
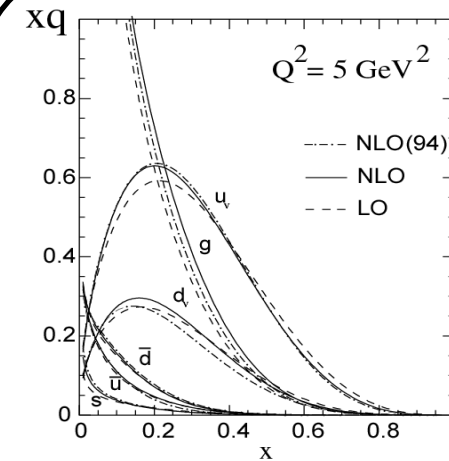


A unified description of partons (quarks and gluons) in the momentum and impact parameter space



Elastic form factors

Transverse spatial distributions

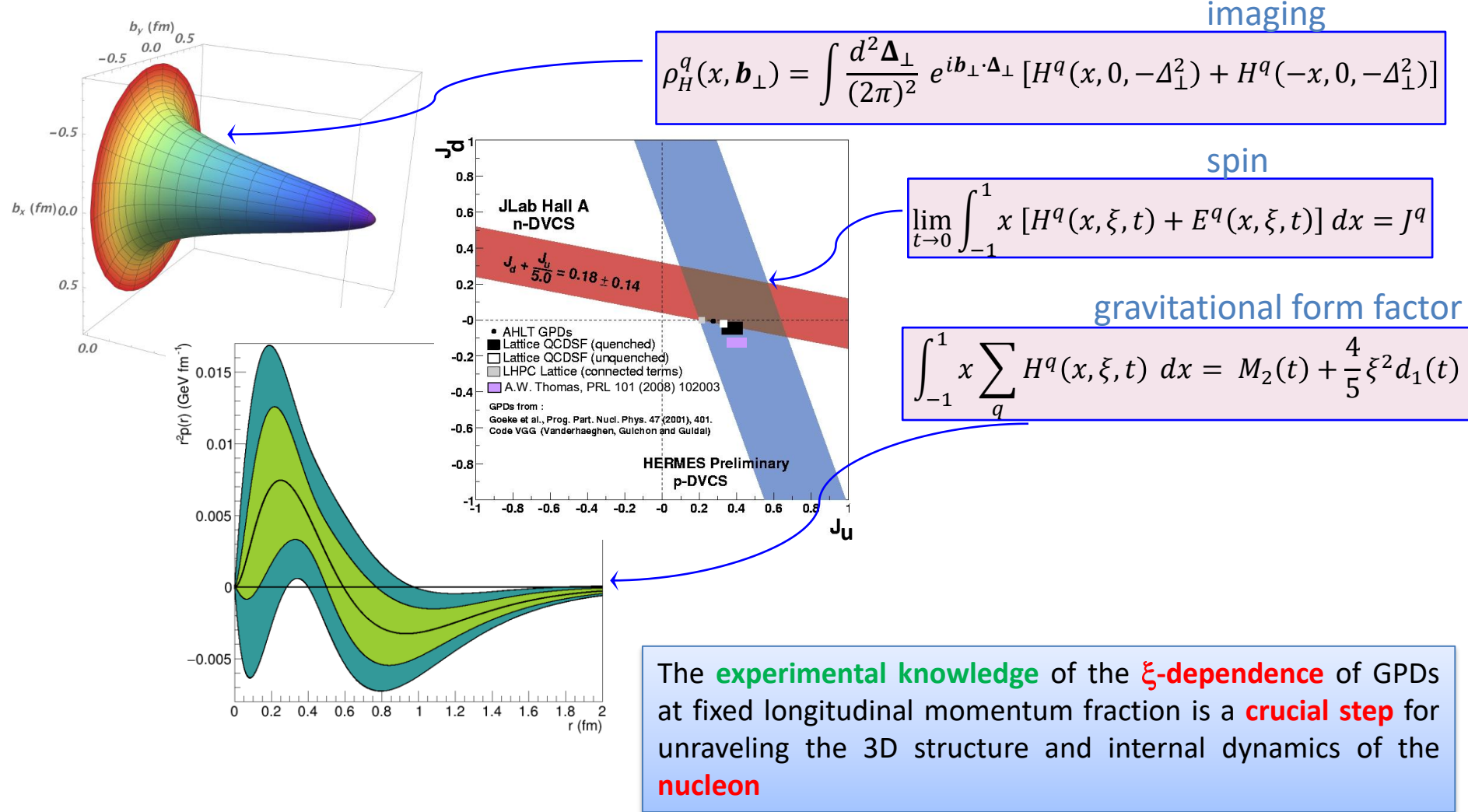


Parton Distribution Functions

Longitudinal momentum distributions

Nucleon Structure and GPD

GPDs encode correlations between partons and contain information about internal dynamics of hadrons like angular momentum or distribution of the forces experienced by quarks and gluons



General Compton Process accessing GPD

$$\gamma^*(q) + p(p) \rightarrow \gamma^*(q') + p(p')$$

$$Q^2 = -q^2, \quad Q'^2 = q'^2, \quad s = (p+q)^2, \quad t = \Delta^2,$$

DVCS	$(\gamma^* \rightarrow \gamma, Q'^2=0, \xi' = \xi)$
Timelike CS	$(\gamma \rightarrow \gamma^*, Q^2=0, \xi' = -\xi)$
Double DVCS	$(\gamma^* \rightarrow \gamma^*, Q^2 Q'^2 \xi' \xi \text{ vary})$

Because of the virtuality of the initial and final photon, **DDVCS** allows direct access to GPDs at $|x| < \xi$, crucial for modeling and investigation of **nuclear imaging, spin, and internal dynamics**

Compton Form Factor (CFF)

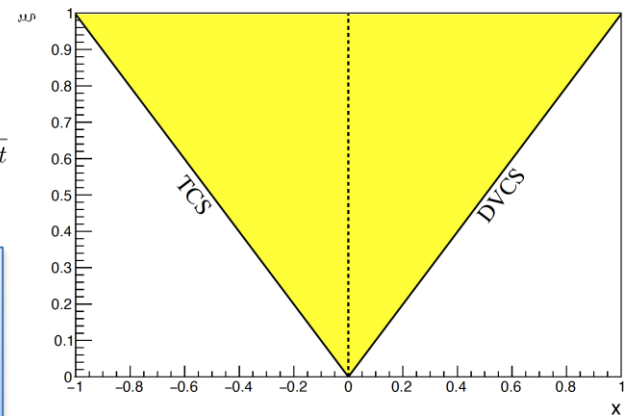
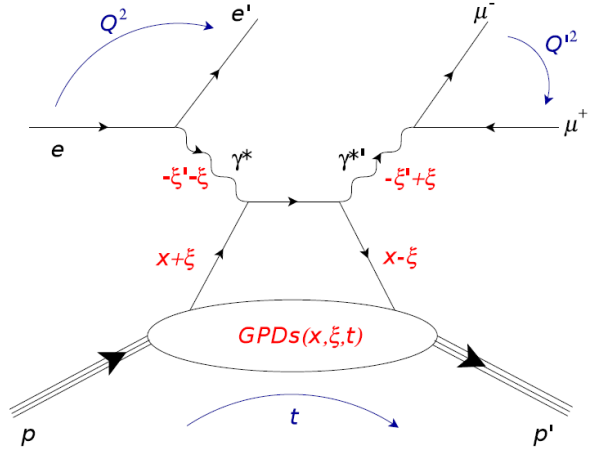
$$\mathcal{F}(\xi', \xi, t) = \mathcal{P} \int_{-1}^1 F_+(x, \xi, t) \left[\frac{1}{x - \xi'} \pm \frac{1}{x + \xi'} \right] dx - i\pi F_+(\xi', \xi, t)$$

GPD combination

$$F_+(x, \xi, t) = \sum_q \left(\frac{e_q}{e} \right)^2 [F^q(x, \xi, t) \mp F^q(-x, \xi, t)]$$

$$\text{Generalized Bjorken variable } \xi' = \frac{Q^2 - Q'^2 + t/2}{2Q^2/x_B - Q^2 - Q'^2 + t} \quad \text{Skewness } \xi = \frac{Q^2 + Q'^2}{2Q^2/x_B - Q^2 - Q'^2 + t}$$

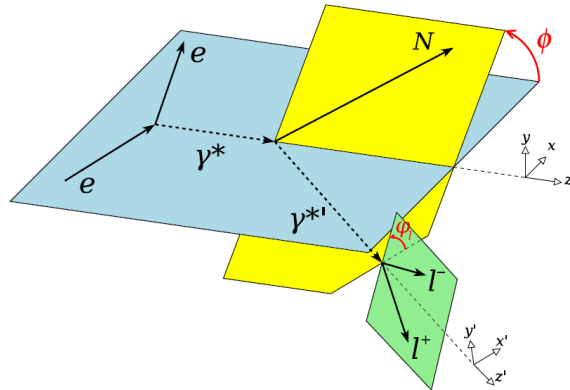
Following the sign change of ξ' around $Q'^2 = Q^2$, the imaginary part of \mathcal{H} and \mathcal{E} **change sign**, providing a testing ground of **GPD universality**.



Elementary Cross Section

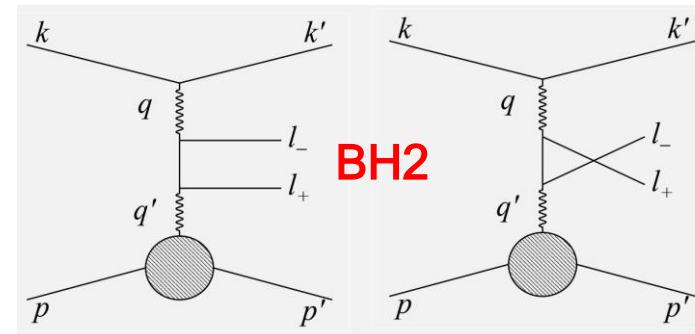
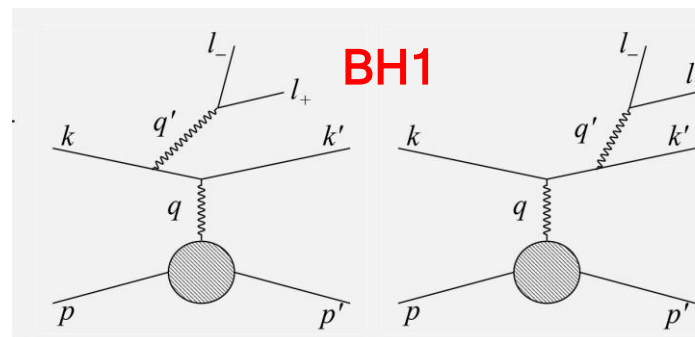
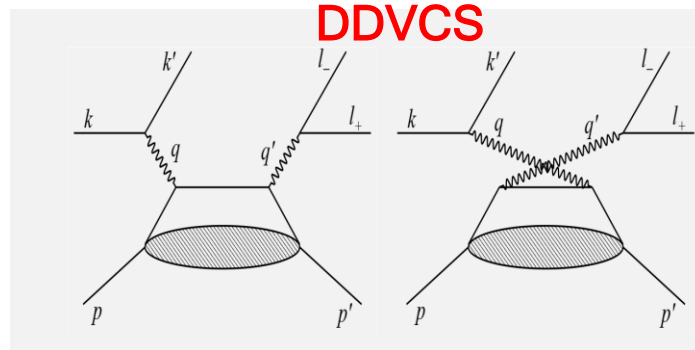
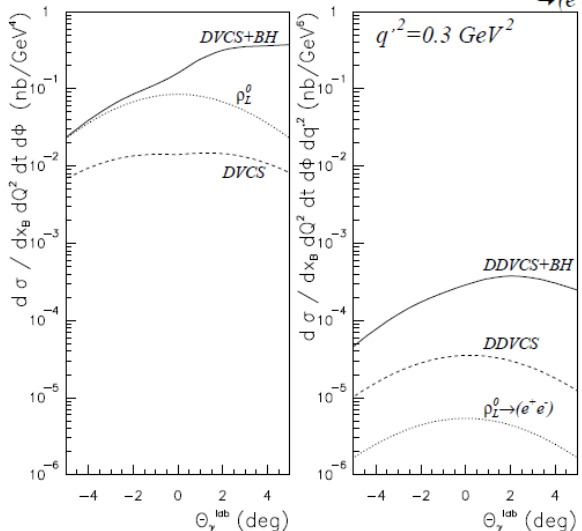
DDVCS cross section is about $\sim 1/100$ of DVCS, involves two Bethe-Heitler (BH) processes

$$d^7\sigma_P^e = d^7\sigma_{BH_1} + d^7\sigma_{BH_2} + d^7\sigma_{DDVCS} + \textcolor{blue}{P} d^7\tilde{\sigma}_{DDVCS} + d^7\sigma_{INT_2} + \textcolor{blue}{P} d^7\tilde{\sigma}_{INT_2} - e [d^7\sigma_{BH_{12}} + d^7\sigma_{INT_1} + \textcolor{blue}{P} d^7\tilde{\sigma}_{INT_1}]$$



$$E_e = 6 \text{ GeV}, Q^2 = 2.5 \text{ GeV}^2, x_B = 0.3, \Phi = 0 \text{ deg.}$$

$$e^- + p \rightarrow e^- + p + \gamma, \rho_L^\theta \quad e^- + p \rightarrow e^- + p + (\gamma, \rho_L^\theta) \rightarrow (e^- e^+)$$



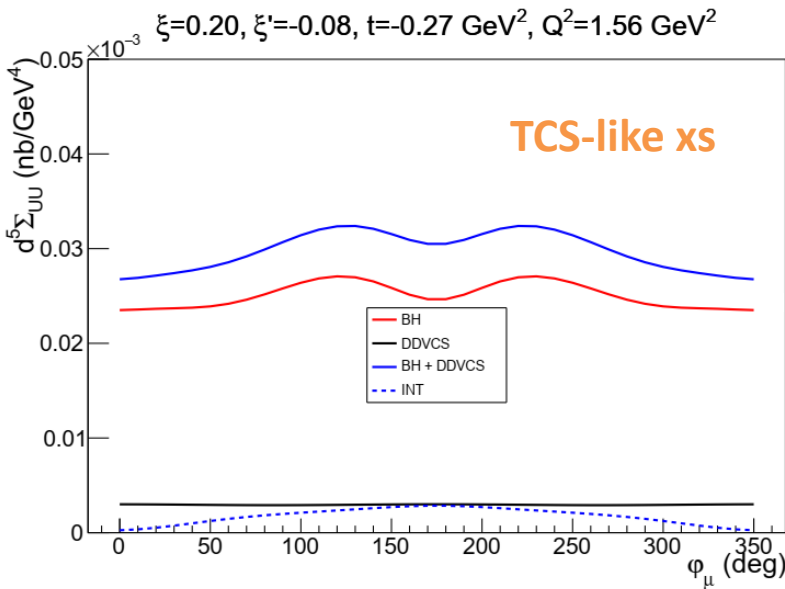
Integrated Cross Section

5-fold TCS-like observables obtained from the integration over the polar angle of muon and the azimuthal angle of initial virtual photon, also minimizing the contribution of the BH₂ process

$$d^5\Sigma^\lambda(\varphi_\mu) \equiv \frac{d^5\sigma^\lambda(\varphi_\mu)}{dx_B dy dt dQ'^2 d\varphi_\mu} = \int_0^{2\pi} d\phi \int_{\pi/2-\theta_0}^{\pi/2+\theta_0} d\theta_\mu \sin(\theta_\mu) \frac{d^7\sigma^\lambda(\phi, \theta_\mu, \varphi_\mu)}{dx_B dy dt d\phi dQ'^2 d\Omega_\mu}$$

$\theta_0 = \pi/4$

$$d^5\Sigma^\lambda = d^5\Sigma_{BH_1} + d^5\Sigma_{BH_2} + d^5\Sigma_{BH_{12}} + d^5\Sigma_{DDVCS} + d^5\Sigma_{\mathcal{I}_1} + d^5\Sigma_{\mathcal{I}_2} + \lambda d^5\tilde{\Sigma}_{\mathcal{I}_2} = d^5\Sigma_{UU} + \lambda d^5\Sigma_{LU}$$



- Our study focuses on using TCS-like observables for projection to allow access to both terms above
- DVCS-like observables obtained by integrating over muon phi angle may also be considered as crosscheck

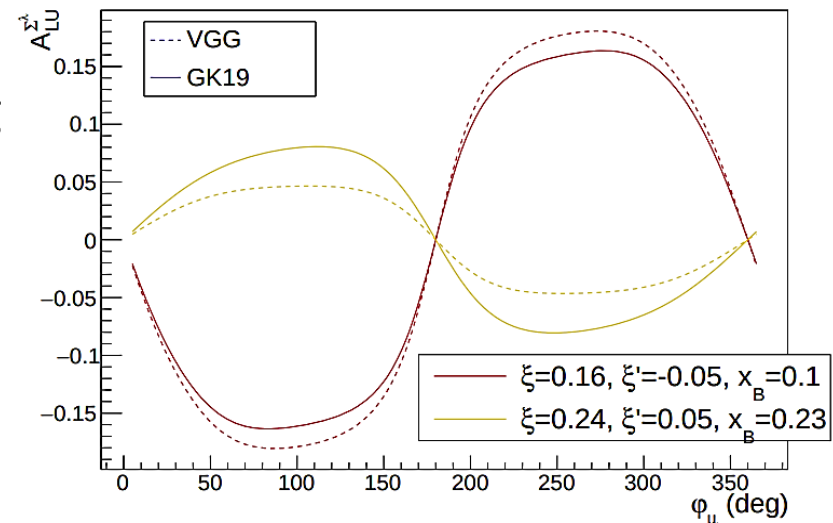
Beam Spin Asymmetry

$$A_{LU}^{\Sigma^\lambda}(\varphi_\mu) = \lambda \frac{d^5\Sigma^+ - d^5\Sigma^-}{d^5\Sigma^+ + d^5\Sigma^-} = \frac{\lambda d^5\tilde{\Sigma}_{\mathcal{I}_2}}{d^5\Sigma_{BH_1} + d^5\Sigma_{BH_2} + d^5\Sigma_{BH_{12}} + d^5\Sigma_{DVCS} + d^5\Sigma_{\mathcal{I}_1} + d^5\Sigma_{\mathcal{I}_2}}$$

$$\propto \text{Im} \left\{ F_1 \mathcal{H} + \xi' (F_1 + F_2) \tilde{\mathcal{H}} - \frac{t}{4M_N^2} F_2 \mathcal{E} \right\}$$

- Access to the imaginary part of CFFs
- **BSA** changes sign when transitioning from **DVCS-like region** ($\xi' > 0, Q^2 > Q'^2$) to **TCS-like region** ($\xi' < 0, Q^2 < Q'^2$)
- **DDVCS BSAs** are dominated by the CFF \mathcal{H} , thus providing a measurement of the \mathcal{H} GPD at $\xi' \neq \pm \xi$ with similar quality to DVCS

BSA in two regions



Muon Charge Asymmetry

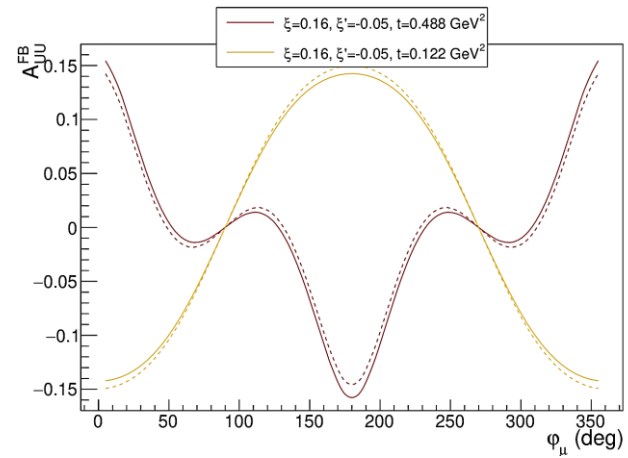
$$A_{UU}^{\mu\pm}(\varphi_\mu) = \frac{d^5\Sigma_{UU}(\varphi_{\mu-}) - d^5\Sigma_{UU}(\varphi_{\mu+})}{d^5\Sigma_{UU}(\varphi_{\mu-}) + d^5\Sigma_{UU}(\varphi_{\mu+})}$$

$$= \frac{d^5\Sigma_{BH_{12}} + d^5\Sigma_{\mathcal{I}_2}}{d^5\Sigma_{BH_1} + d^5\Sigma_{BH_2} + d^5\Sigma_{DDVCS} + d^5\Sigma_{\mathcal{I}_1}}$$

$$d^5\Sigma_{\mathcal{I}_2} \propto -\frac{\xi'}{\xi} \Re e \left[F_1 \mathcal{H} + \frac{\xi^2}{\xi'} (F_1 + F_2) \tilde{\mathcal{H}} - \frac{t}{4M_N^2} F_2 \mathcal{E} \right]$$

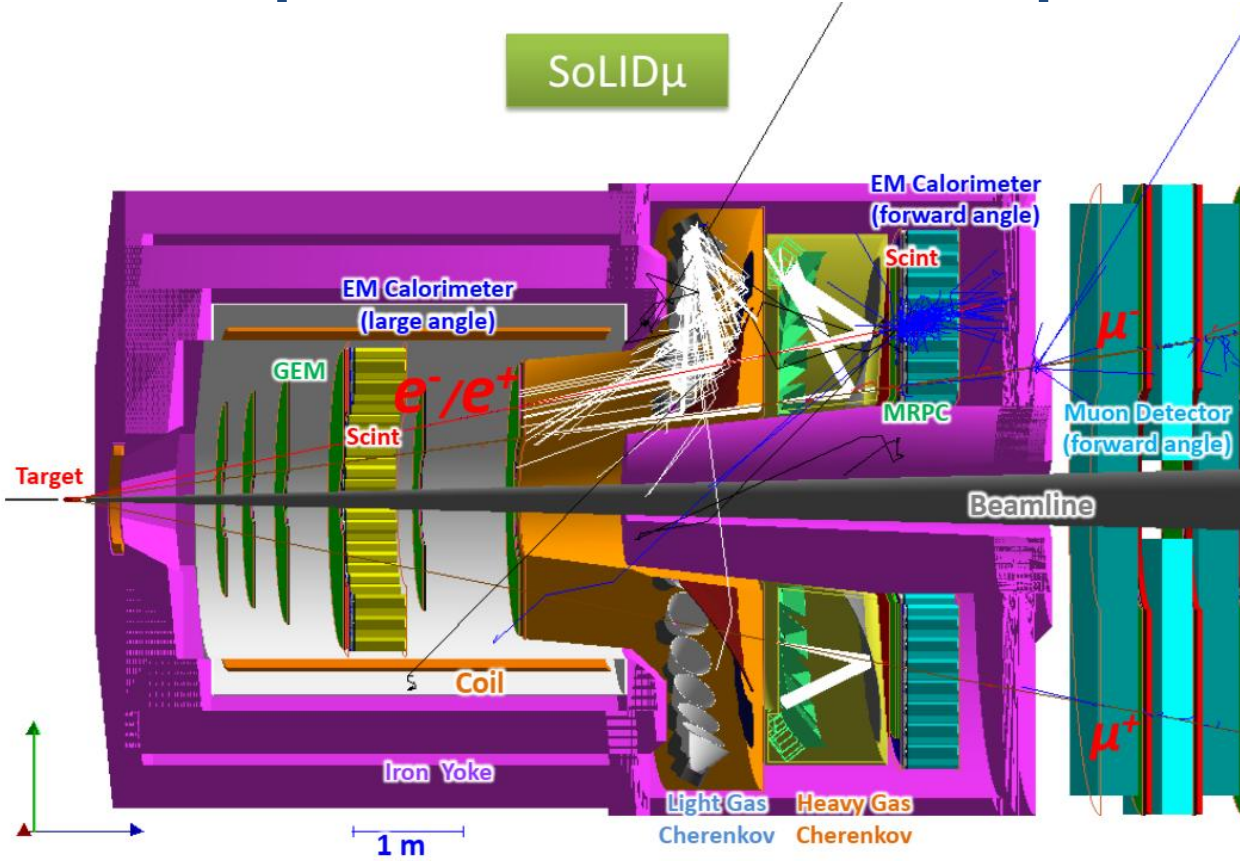
aka Forward Backward Asymmetry

μCA in two regions



- Access to the real part of CFFs (no dispersion relation has been established)
- **μCA** predicted to have **significant amplitude** and rich **harmonic composition**, like the forward-backward asymmetry of TCS
- **Curvature change** is a highly-discriminating feature for models
- **DDVCS μCA** access a CFF combination **different from BSA**. This feature **distinguishes DDVCS** from DVCS and TCS.

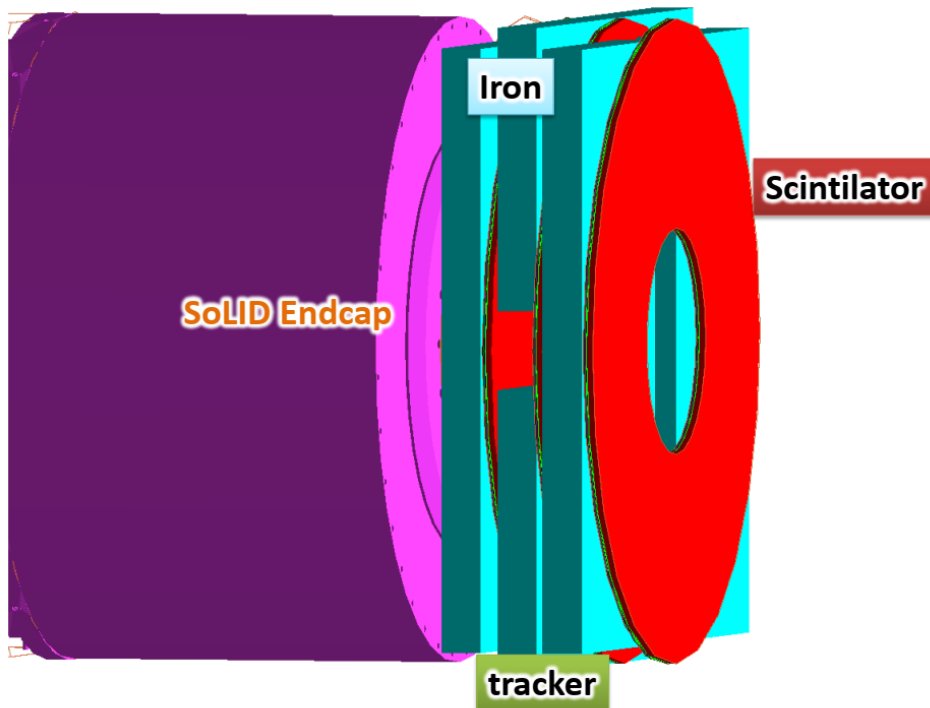
Experimental Setup



- SoLID can detect e^- , e^+ , proton, pion
- Based on SoLID J/Psi and TCS setup ($1.2e37/cm^2/s$) with forward angle muon detector added to form **SoLIDμ spectrometer**
- **Sharing** beam time with approved J/Psi and TCS di-e experiment
- Forward Angle (FA) covers 8.5-16.5deg and Large Angle (LA) covers 18-30deg

Forward Angle Muon Detector (FAMD)

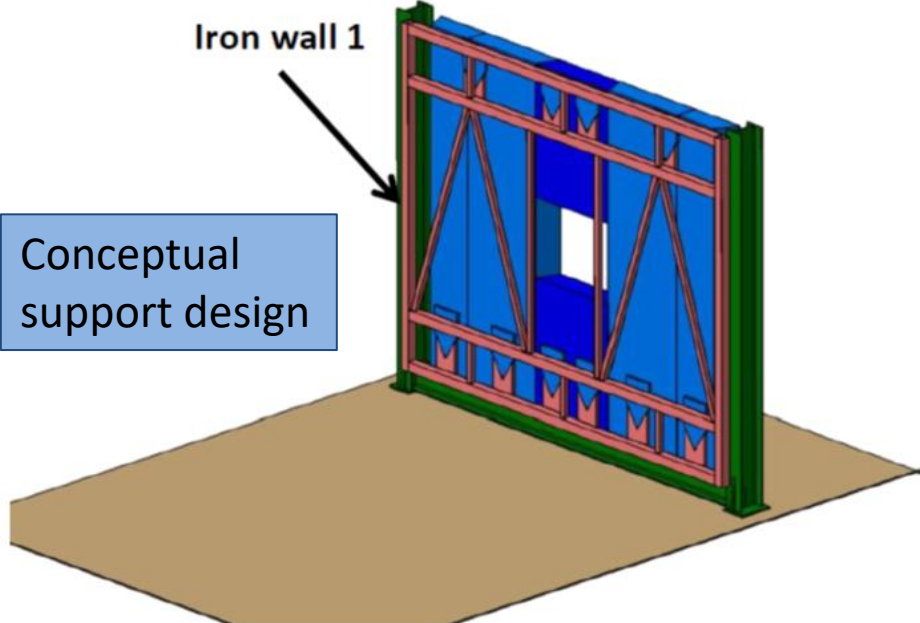
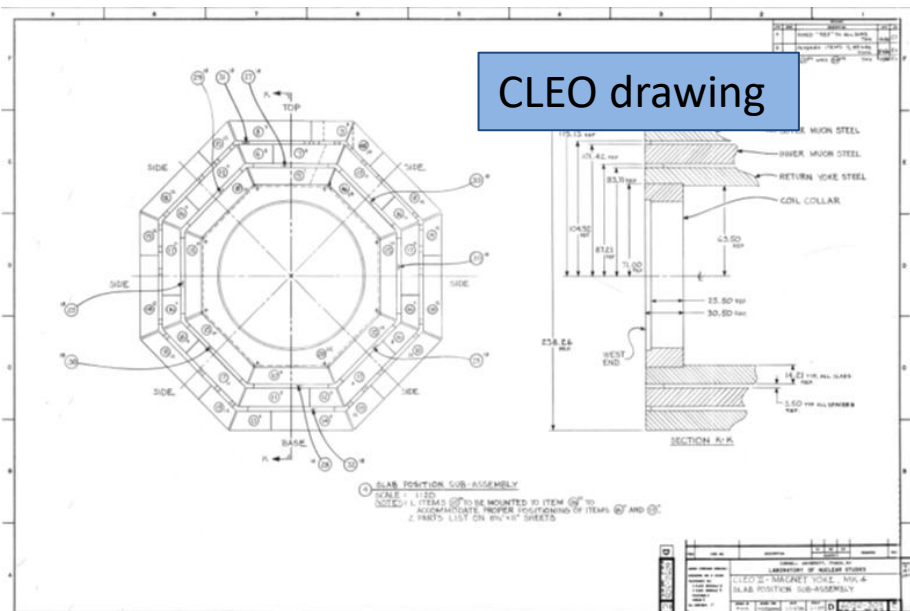
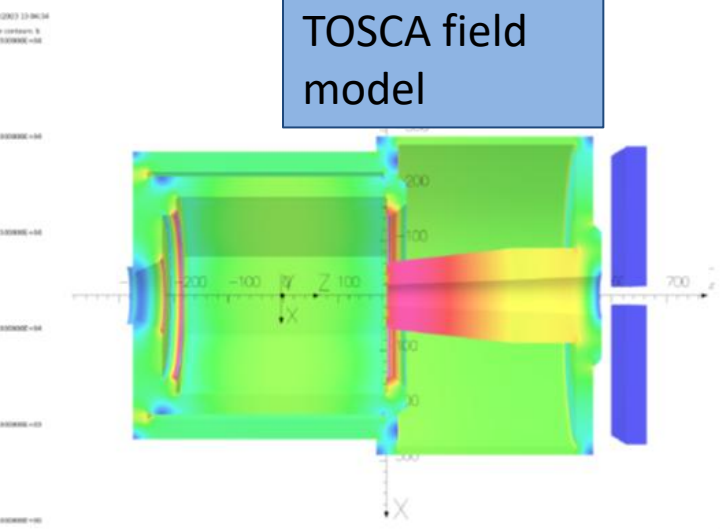
Forward Angle Muon Detector



- 3 layers of iron+tracker+scintillator ($R_{in}=1m$, $R_{out}=3m$)
- Iron for pion blocking
- μ RWell trackers to connect with tracks in SoLID inner GEM trackers
 - track resolution from SoLID inner trackers only
- scintillators for muon PID with pion suppression and trigger

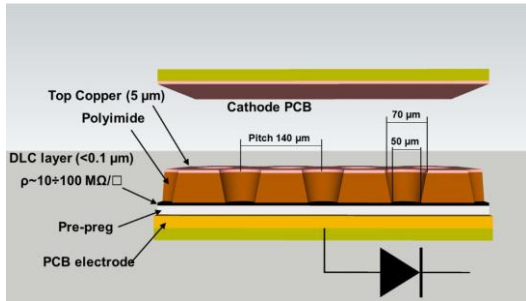
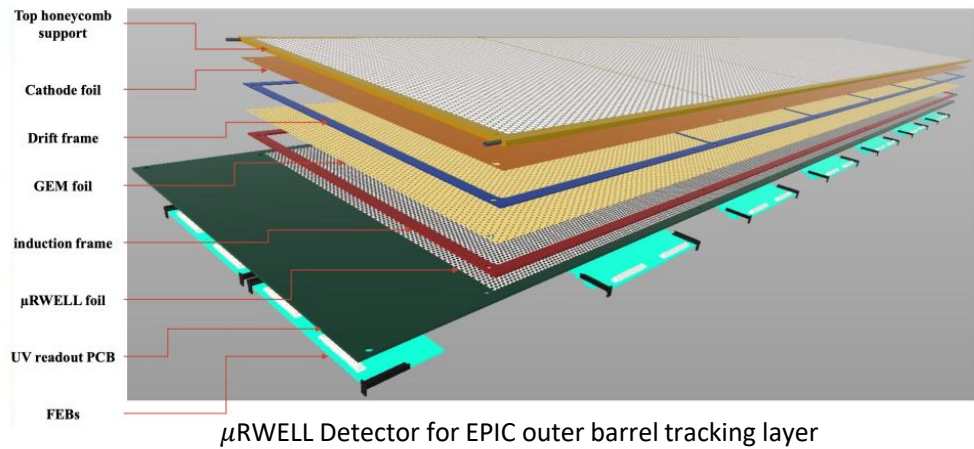
Iron of FAMD

- Reuse 6 of CLEO octagon outer layer iron
- Each one is about 36x254x533cm
- No problem with space
- Field (<10G), force(<1N), torque(<2Nm) are small

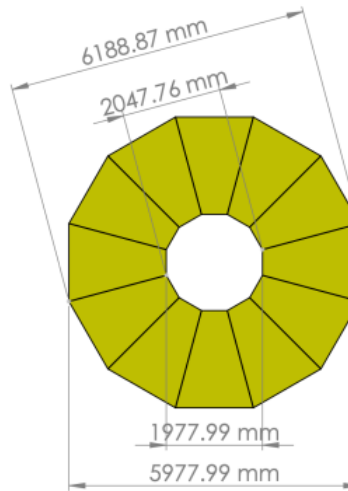


μ RWell trackers of FAMD

- μ RWell tracker with good rate capability and lower cost than GEM
- VMM electronics for readout
- 2D UV strips with capacitive charge sharing to have rate 30KHz/cm² and position resolution of 1 mm



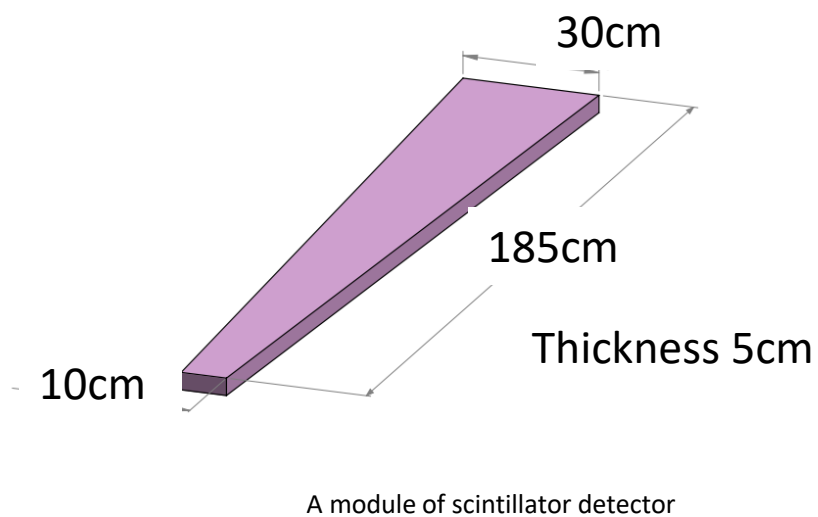
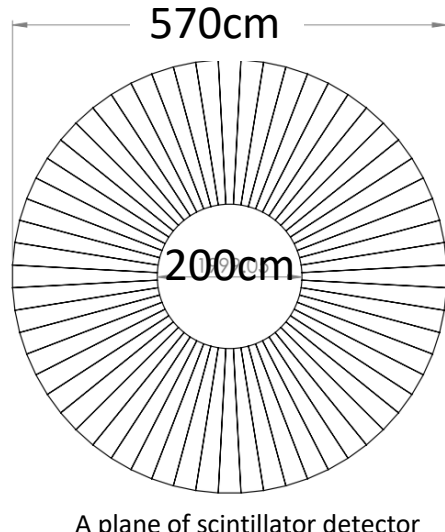
μ RWELL Detector – G. Bencivenni *et al* 2019 JINST **14** P05014



A plane of μ RWell detector

Scintillators of FAMD

- 3 layers of scintillator planes
- Each plane has 60 azimuthal segments
- Readout with light guide and PMTs from both inner and outer radial ends
- Design similar to CLAS12 forward scintillator and SoLID large angle scintillator with similar performance

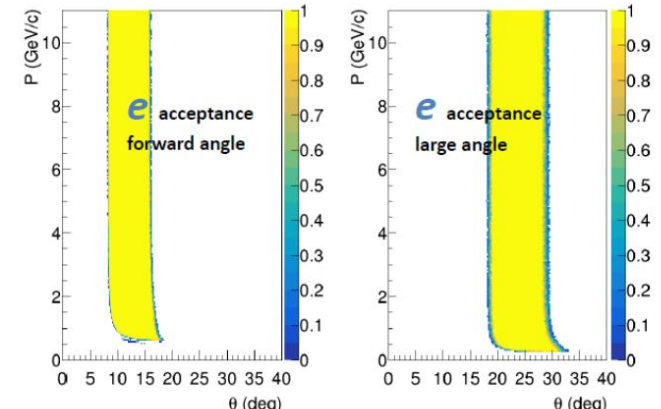
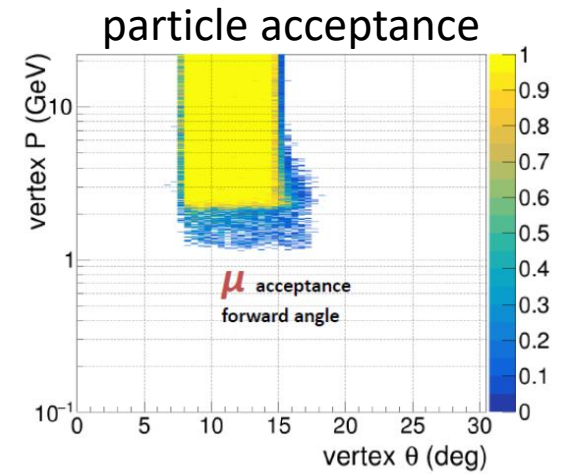
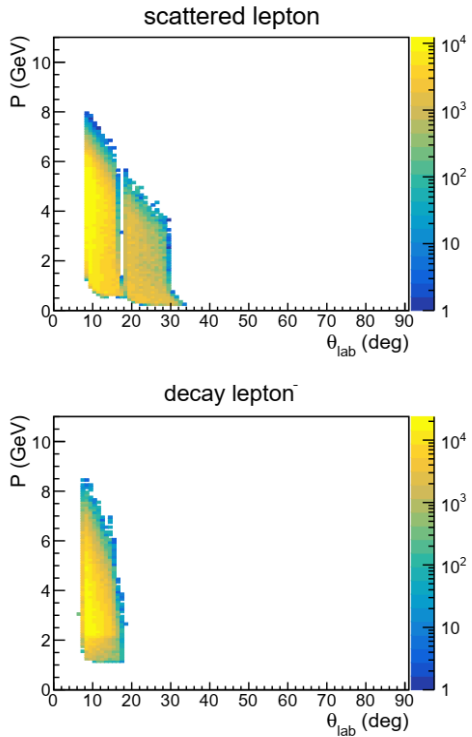


Event Acceptance

BH generator "grape-dilepton" used by HERA and verified by CLAS12

- Best topology 3-fold(e+mu+mu): scattered e- at FA+LA, both muons at FA, proton not detected
- Additional topology 4-fold(e+mu+mu+p): recoil proton at FA+LA (clean)

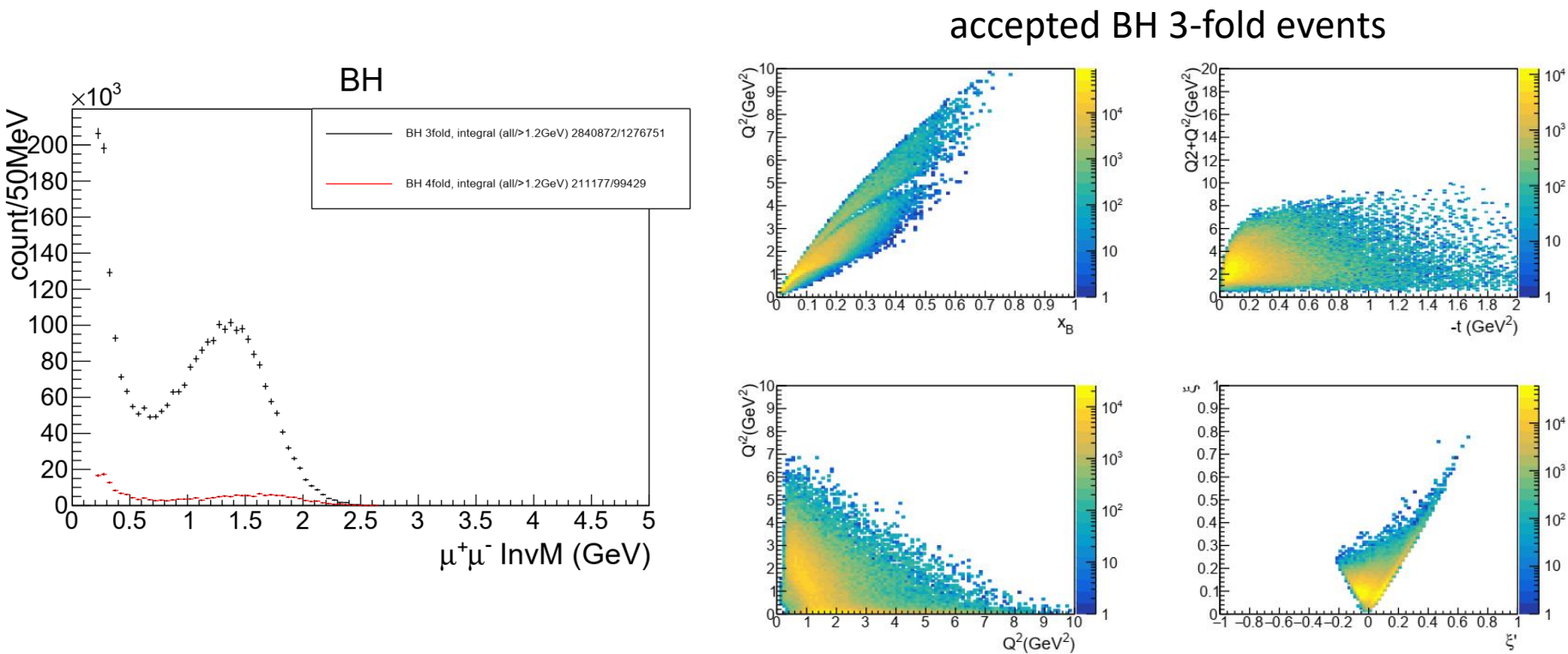
accepted BH 3-fold events



- full azimuthal coverage and large acceptance
- Solenoid field helps control systematics

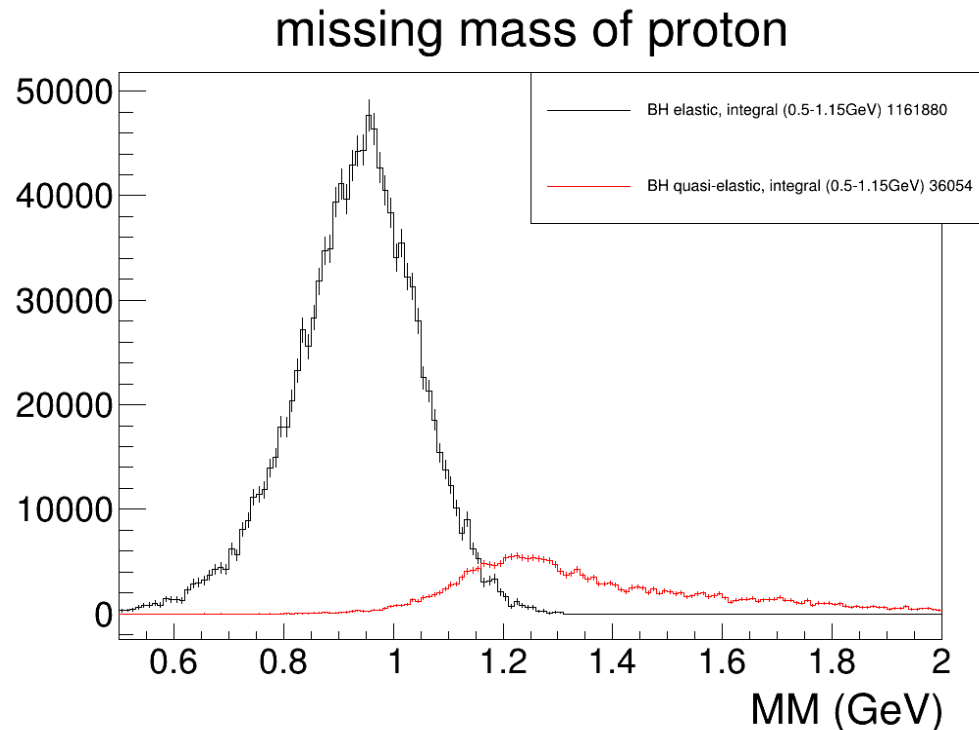
Event Distribution

- 3-fold BH events covers a large kinematic range
- 0.7 overall detection efficiency
- Enough counts with $1.2\text{e}37/\text{cm}^2/\text{s}$ luminosity and 100 days to have multidimensional binning



Exclusivity cut

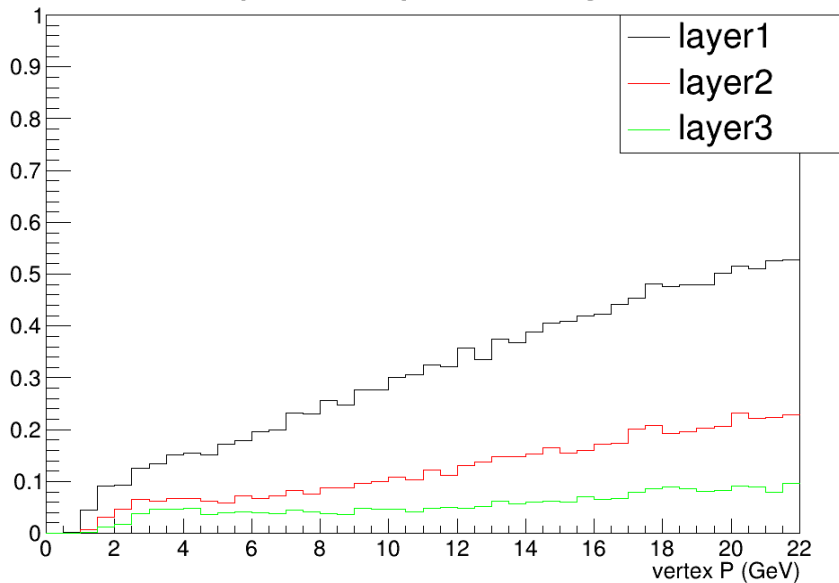
- Both BH with 4 final particles (elastic) and more than 4 particles (quasi-elastic), generated by "grape-dilepton"
- Missing proton mass of 3 fold BH events with resolution from SoLID inner GEM trackers, for resonance free region (muon pair InvM>1.2GeV)
- **3-4% background** after cutting MM>1.15GeV



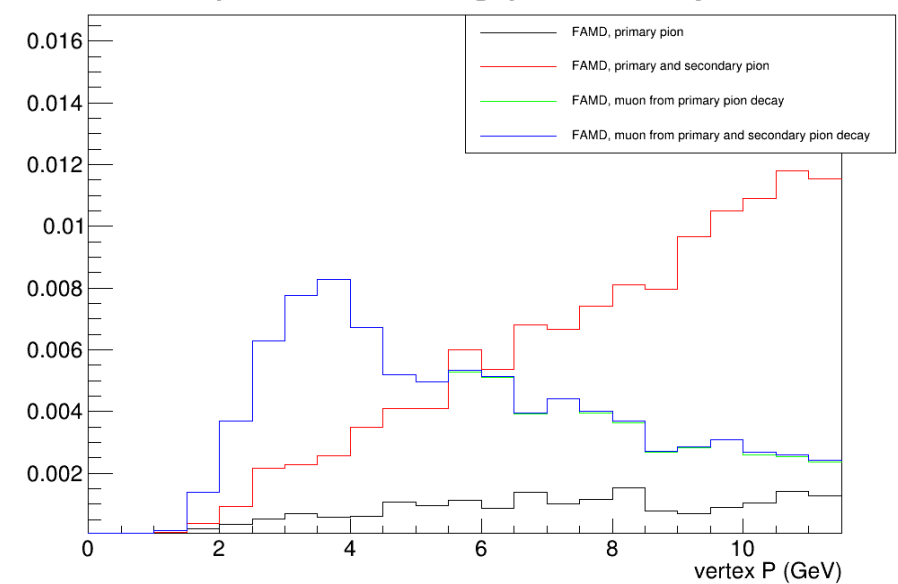
Pion blocking

- Geant4 simulation of pions from target with some probabilities creating hits at FAMD
- "pion hit probability", hits of charged particles entering each layer, used for FAMD background and trigger rate estimate
- "pion surviving probability", hits of pion and muon at the last layer of FAMD with tracks passing all SoLID inner GEM trackers, used for physics event rate estimation

pion hit probability

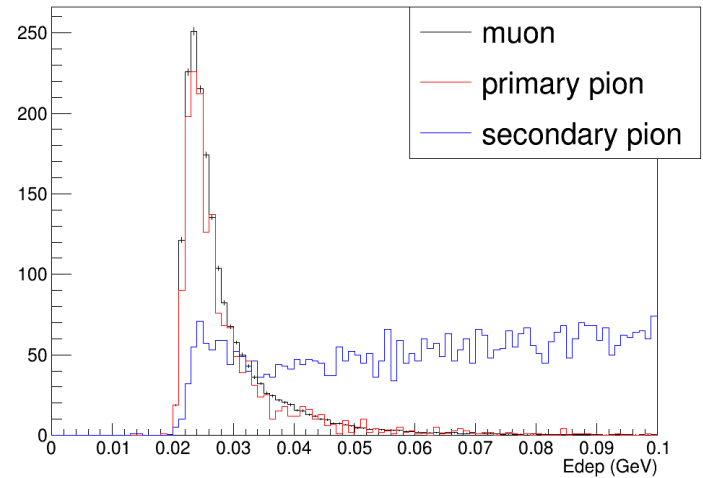
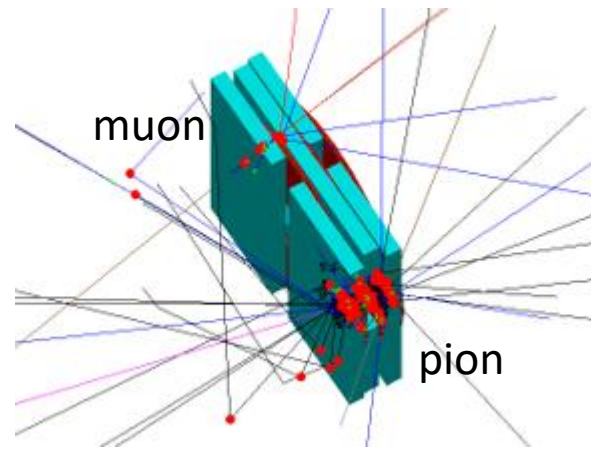


pion surviving probability



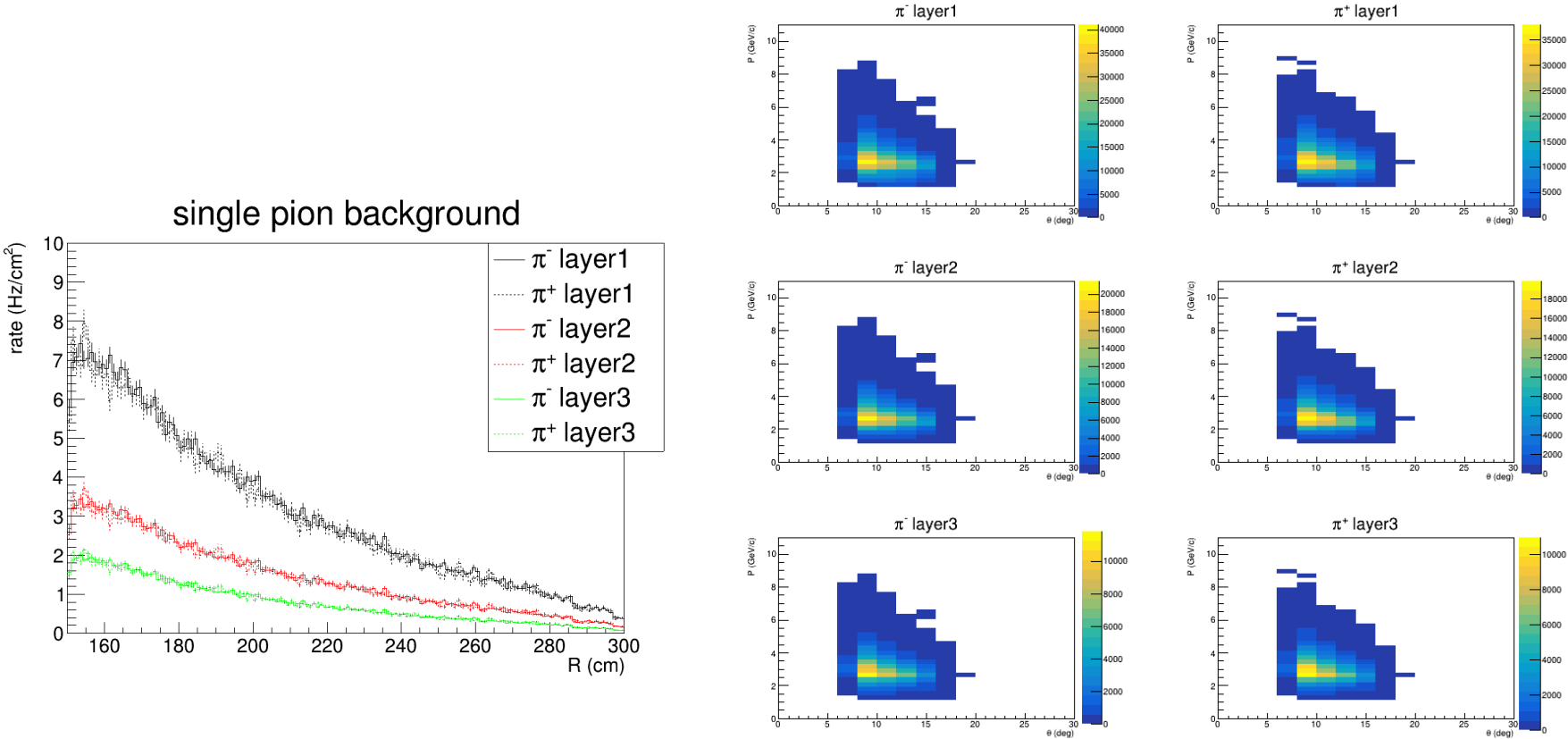
Pion suppression within FAMD

- Muons behave as Minimum Ionizing Particle (MIP)
- Pions often deposit more energy over 3 layers of scintillators.
- Use a moderate pion suppression factor 2 from energy cut



Single pion background

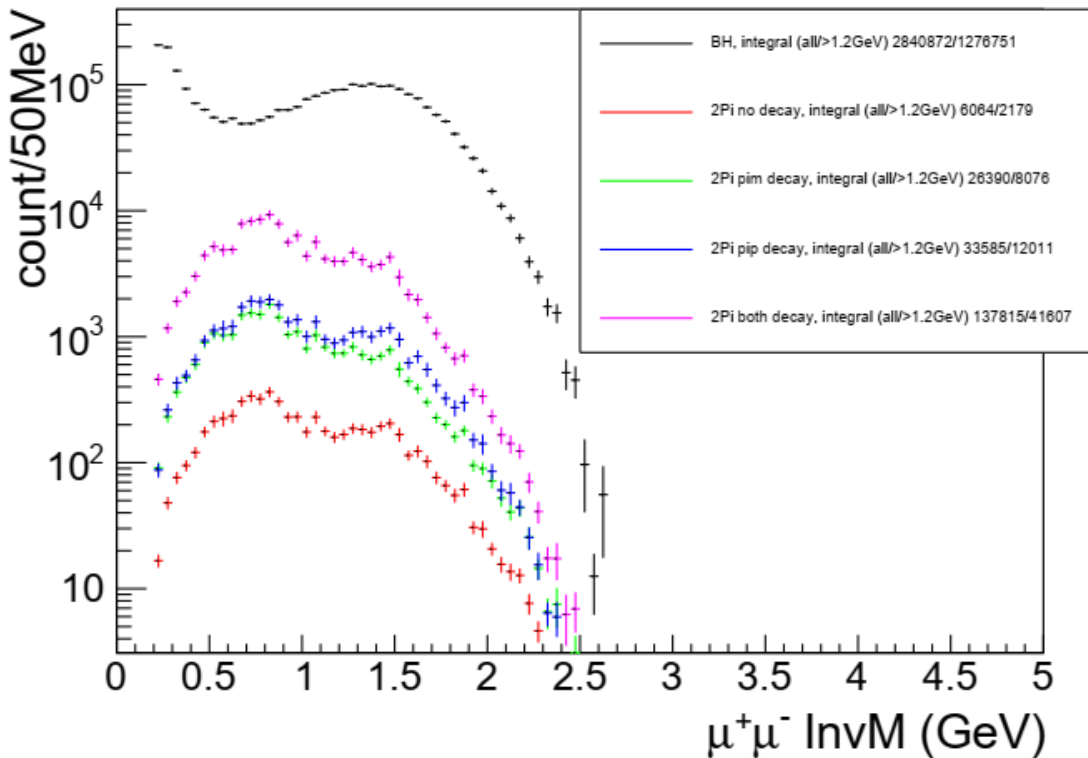
- Combining single pion generator "evgen_bggen" (pythia+MAID) events with "pion hit probability", study charged particle rate at 3 layers. Full simulation confirmed the result
- Single particle trigger 600kHz rate with hits in all 3 layers of scintillators in nearby phi sectors
- Coincidence of two hits from 2 single particle trigger from 2 different phi sectors within 50ns time windows leads to **18khz final trigger rate**
- Fake coin rate from single pion is below 1khz. BH di-muon events have two muons separated at least by 60 degrees in phi angle for the main physics region (muon pair InvM>1.2GeV)



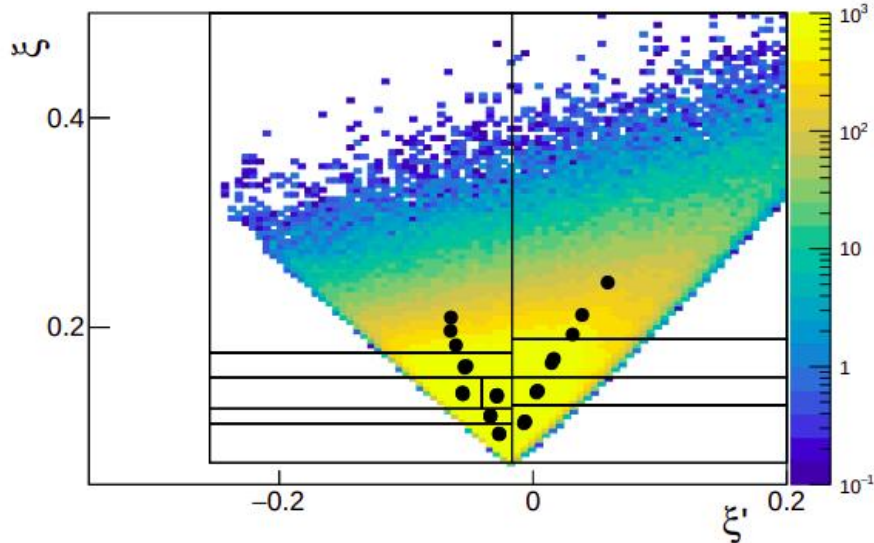
Two pion exclusive background

- Main physics background from two pion exclusive channel (missing mass cut won't reject it because pions and muons have similar mass)
- Combine event generator "twopeg" (fit to CLAS data) and "pion hit probability" with pion suppression factor 2, study "2pi" rate and compare to BH rate
- **5-7% background**, while the channel be measured by the internal SoLID detector at the same time to control systematics

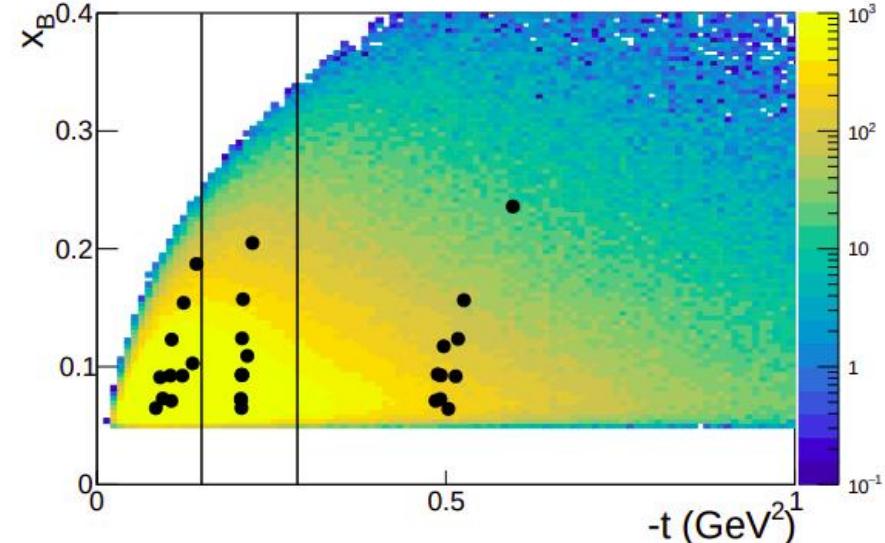
BH and 2pi comparison



Experimental projection binning



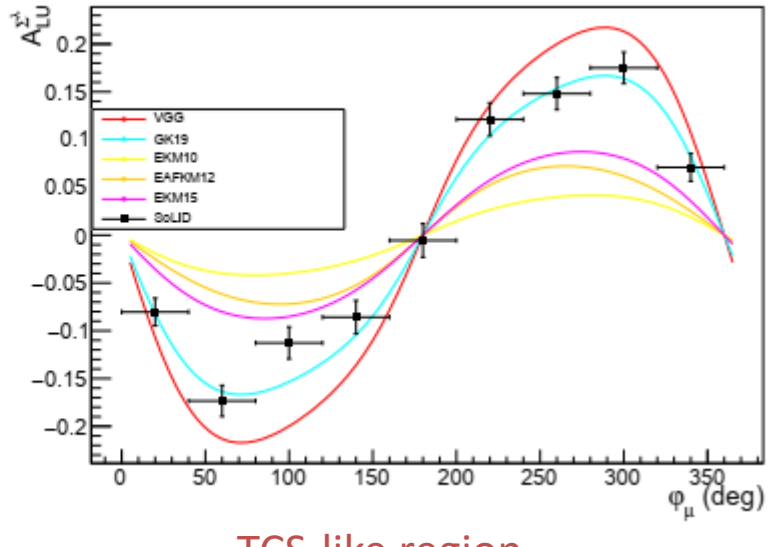
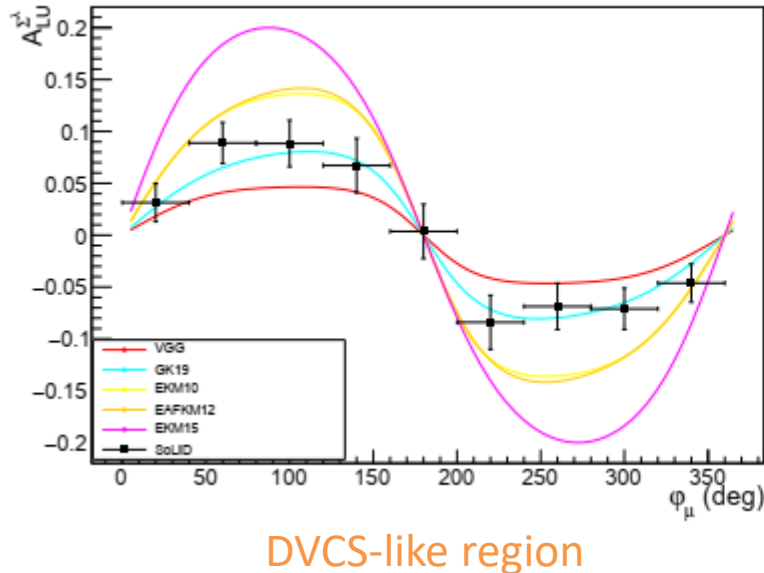
(a) (ξ', ξ) space.



(b) $(-t, x_B)$ space.

- 100 days would allow for measurements on a five-dimensional grid ($\xi' \xi t x_B \Phi_\mu$)
- Covers both DVCS-like region ($\xi' > 0, Q^2 > Q'^2$) to TCS-like region ($\xi' < 0, Q^2 < Q'^2$)

BSA experimental projections



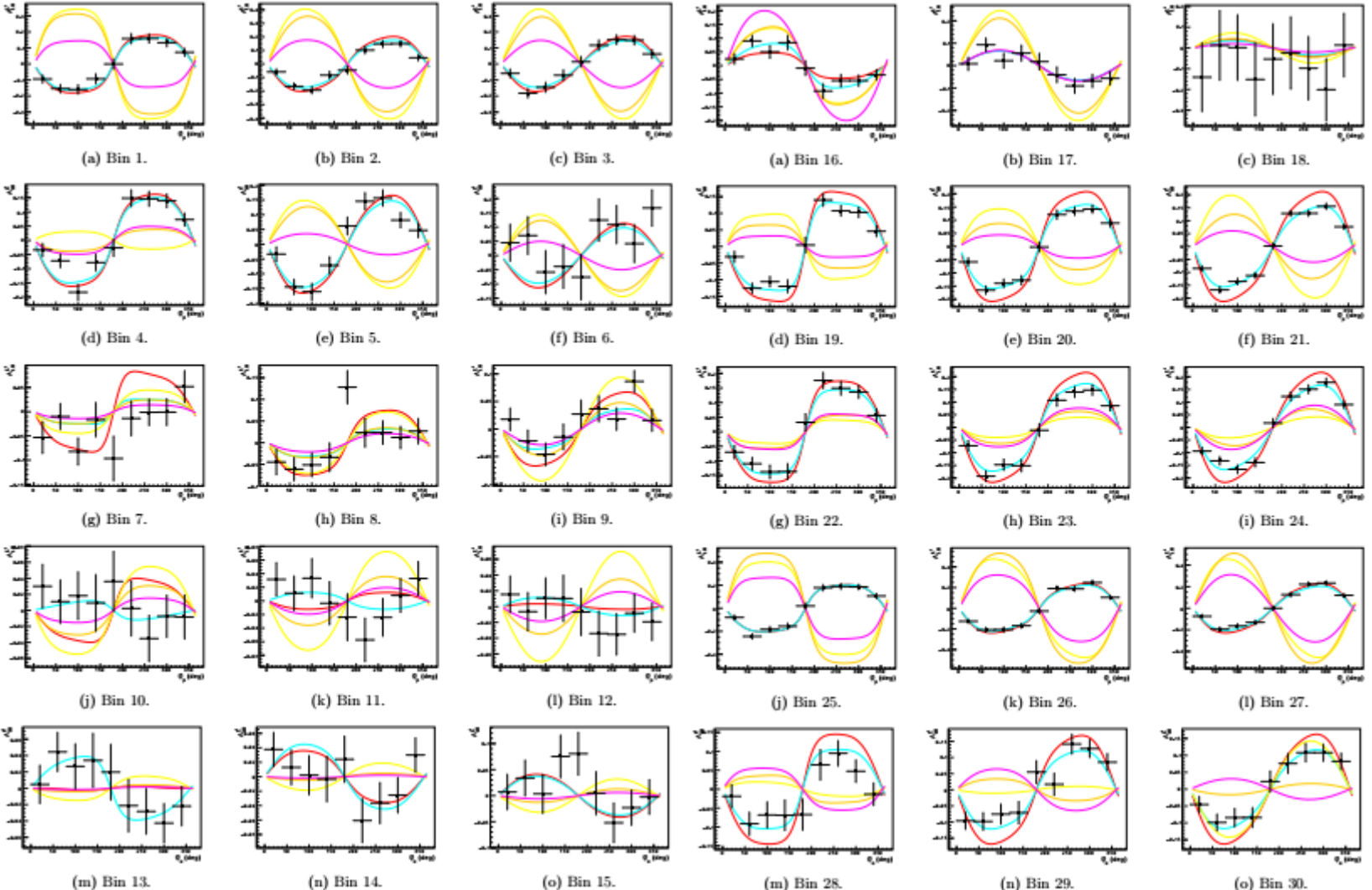
arXiv:2502.02346

- First time measurement of the BSA sign change between the two regions
- Possibility to constrain GPD models

All projection plots include statistical and polarization errors

BSA experimental projections

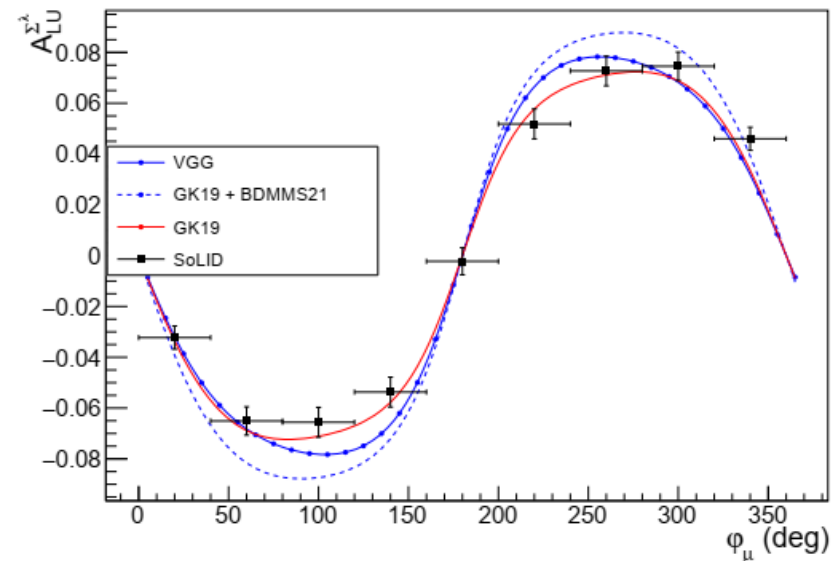
All plots over the entire kinematic range



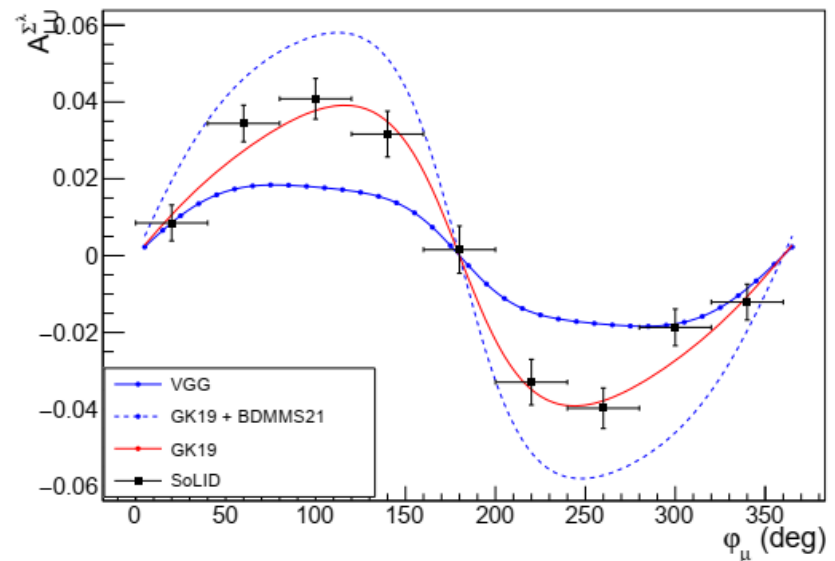
Bin	ζ' range	ζ range	t range (GeV)
1	$-0.255 < \zeta' < 0$	$0.152 < \zeta < 0.176$	$-5.541 < t < -0.257$
2			$-0.287 < t < -0.150$
3			$-0.150 < t < -0.020$
4		$0.176 < \zeta < 0.739$	$-5.541 < t < -0.257$
5			$-0.287 < t < -0.150$
6			$-0.150 < t < -0.020$
7	$0 < \zeta' < 0.512$	$0.071 < \zeta < 0.124$	$-5.541 < t < -0.257$
8			$-0.287 < t < -0.150$
9			$-0.150 < t < -0.020$
10		$0.126 < \zeta < 0.153$	$-0.287 < t < -0.150$
11			$-0.287 < t < -0.150$
12			$-0.150 < t < -0.020$
13		$0.153 < \zeta < 0.189$	$-5.541 < t < -0.257$
14			$-0.287 < t < -0.150$
15			$-0.150 < t < -0.020$
16		$0.189 < \zeta < 0.739$	$-5.541 < t < -0.257$
17			$-0.287 < t < -0.150$
18			$-0.150 < t < -0.020$
19	$-0.255 < \zeta' < -0.017$	$0.071 < \zeta < 0.108$	$-5.541 < t < -0.257$
20			$-0.287 < t < -0.150$
21			$-0.150 < t < -0.020$
22		$0.108 < \zeta < 0.127$	$-5.541 < t < -0.257$
23			$-0.287 < t < -0.150$
24			$-0.150 < t < -0.020$
25	$-0.255 < \zeta' < -0.040$	$0.122 < \zeta < 0.152$	$-5.541 < t < -0.257$
			$-0.287 < t < -0.150$
			$-0.150 < t < -0.020$
	$t < \zeta' < -0.017$	$0.122 < \zeta < 0.152$	$-5.541 < t < -0.257$
			$-0.287 < t < -0.150$
			$-0.150 < t < -0.020$

Bin boundaries of the binning scheme shown in Fig. 24

BSA experimental projections



(a) $-0.1 < \xi' < -0.04$.

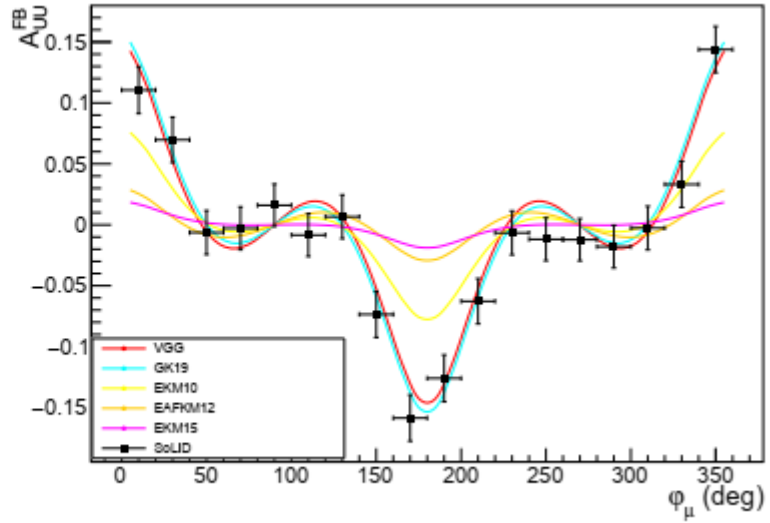
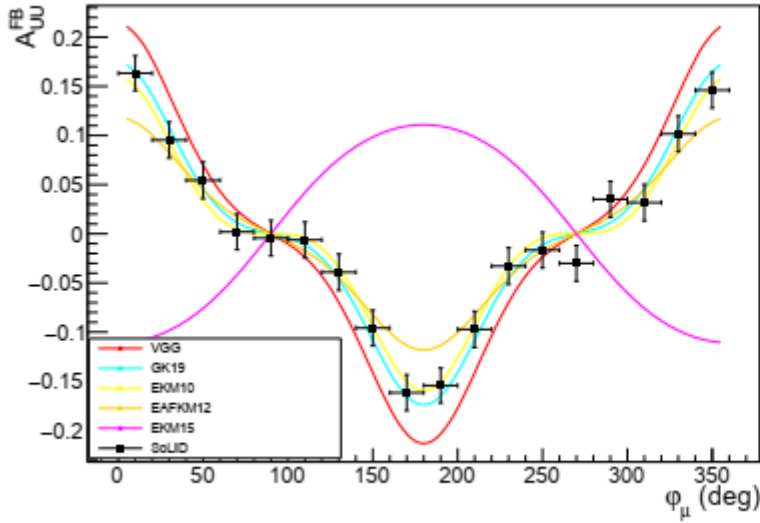


(b) $-0.04 < \xi' < 0.1$.

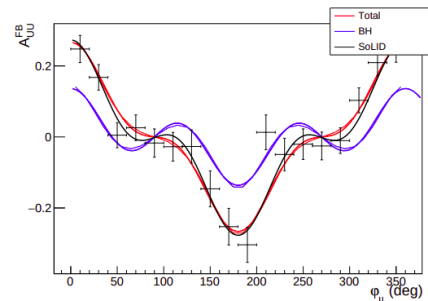
Figure 26: Projected exploratory TCS-like BSA measurements sensitive to shadow GPDs in the $0.3 < \xi < 0.4$ region.

First time exploratory measurement of BSA constraining shadow GPD models (a class of functions with null CFF and forward limit contributing to GPD solutions in the deconvolution problem)

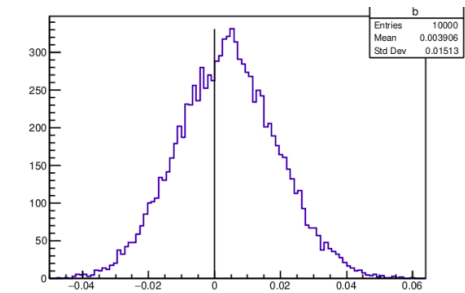
μ CA experimental projections



First time exploratory measurement
of μ CA to access the CFF real part
with curvature change



(a) μ CA and the components entering the $\cos \varphi_\mu$ mo-



(b) Distribution of the $\cos \varphi_\mu$ moment of the μ CA

$$A_{UU}^{\mu\pm}(\varphi_\mu) = a_0 + a_1 \cos(\varphi) + a_3 \cos(3\varphi)$$

- known BH contribution is small in certain regions and can be subtracted
- μ CA has contributions from $\cos(\phi)$ and $\cos(3\phi)$ modulations
- $\cos(\phi)$ component can be extracted from fitting

Systematic effects

BSA systematics originates mainly from electron beam polarization, electron detection efficiency, and muon detection efficiency

$$A_{LU}^{\Sigma\lambda} = \frac{1}{\lambda} \frac{Y_+ - Y_-}{Y_+ + Y_-}$$

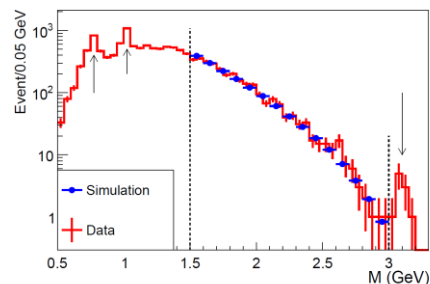
$$Y_{\pm}(\varphi_{\mu}) = \frac{1}{Q_{\pm}} \frac{1}{\Delta\Omega_e(\varphi_{\mu}) \Delta\theta_{\mu}(\varphi_{\mu})} \int_0^{2\pi} d\phi \int_{\pi/4}^{3\pi/4} d\theta_{\mu} \sin(\theta_{\mu}) \frac{N_{\pm}(\varphi_{\mu}, \phi, \theta_{\mu})}{\epsilon_e(\phi) \epsilon_{\mu}(\varphi_{\mu}, \theta_{\mu})}$$

$$Y_{\pm}(\varphi_{\mu}) \equiv \sum_{i=1}^{N_{\phi}} \sum_{j=1}^{N_{\theta_{\mu}}} \frac{n_{\pm}^{ij}}{\epsilon_e^i \epsilon_{\mu}^j}$$

$$\delta A_{LU}^{\Sigma\lambda} = \sqrt{\left[A_{LU}^{\Sigma\lambda}\right]^2 \left(\frac{\delta\lambda}{\lambda}\right)^2 + \frac{1}{2\lambda^2} \frac{1}{N_{\phi}} \left(\frac{\delta\epsilon_e}{\epsilon_e}\right)^2 + \frac{1}{2\lambda^2} \frac{1}{N_{\theta_{\mu}}} \left(\frac{\delta\epsilon_{\mu}}{\epsilon_{\mu}}\right)^2}$$

$\lambda = 0.85 \rightarrow 0.04$

Bin independence hypothesis $(N_{\phi}, N_{\theta_{\mu}})$ are the kinematic dependent number of bins, typically (20,10)



CLAS12 BH di-e data
and sim comparison

Control systematics through reference channels

- SoLID will have crosssection measurement before this experiment
- For e- detection, use inclusive DIS and elastic measurements
- For muon detection, use both resonance and resonance free region and cross check both di-e and di-mu channels
- Pion channel measurement are also taken at the same time

Beam time request

Beam Energy (GeV)	Beam Current (uA)	Beam Requirements	Target Material	Target Thickness (cm)	Beam time (days)
11	3	polarized (>85%)	LH2	15	
Run Group Calibration time					10
Run Group Production time					50
Requested Production time					50
Total Time					110

- Main trigger on di-muon to take DDVCS, J/psi and TCS di-mu data at the same time
- Independent di-e trigger for approved J/psi and TCS di-e data taking at the same time
- **Comprehensive program including muons and electrons within same runs.** It can also help cross check systematics

Summary

This proposed experiment

- complement SoLID J/psi setup with a forward angle **muon detector** to form **SoLID μ spectrometer**
- measure **DDVCS** in the di-muon channel
- **share** approved J/psi beamtime 60 days and request **additional 50 days**

Its physics impact

- **first time measurement** of **DDVCS** (mainly BSA and exploratory μ CA) over a broad kinematic range
- **first time to access GPD** $|x| < \xi$ as input for models and global fitting

Proposal to PAC53 PR12-25-010

Proposal to JLab PAC 53

Double Deeply Virtual Compton Scattering with SoLID μ spectrometer

Xinzhan Bai*, Alexandre Camsonne*†, Silviu Covrig Dusa, Kondo Gnanno, Dave Mack, Michael McCaughan, and Richard Tyson

Thomas Jefferson National Accelerator Facility, Newport News, VA, USA

Juan-Sebastian Alvarado*, Raphaël Dupré, Adam Hobart, Dominique Marchand, Carlos Muñoz Camacho, Silvia Niccolai, and Eric Voutier*

Université Paris-Saclay, CNRS/IN2P3/IJCLab, Orsay, France

Haiyan Gao, Yining Liu, Bo Yu, Yi Yu, Zhiwen Zhao*, and Jingyi Zhou
Duke University, Durham, NC, USA

Keagan Bell, Debaditya Biswas, Marie Boér*, Gyang Chung, Mahmoud Gomina, Arna Ma, and Kemal Tezgin

Virginia Tech, Blacksburg, VA, USA

Garth Huber, Nathan Heinrich, Muhammad Junaid, Vijay Kumar, and Alicia Postuma

University of Regina, Regina, SK, Canada

Ronald Gilman

Rutgers University, Piscataway, NJ, USA

Nilanga Linayage, Huong Thi Nguyen, and Asar Ahmed

University of Virginia, Charlottesville, VA, USA

Yi Wang, Junhuai Xu, Zhihong Ye, Haojie Zhang, and Yaopeng Zhang
Tsinghua University, Beijing, China

Evaristo Cisbani

Istituto Superiore di Sanità, Roma, Italia

Guido Maria Urcioli

INFN, Sezione di Roma1, Roma, Italia

Vincenzo Bellini and Concetta Maria Sutera

Università di Catania, Catania, Italia

Anthony W. Thomas

ARC Special Research Centre for the Subatomic Structure of Matter (CSSM),
University of Adelaide, Adelaide, Australia

Pierre Chatagnon¹, Maxime Defurne¹, Víctor Martínez-Fernández^{1,2}, Hervé Moutarde¹, and Franck Sabatié¹

¹ IRFU, CEA, Université Paris-Saclay, Gif-sur-Yvette, France

² Center for Frontiers in Nuclear Science, Stony Brook University, Stony Brook, NY, USA

Malek Mazouz and Wassim Hamdi

Faculté des Sciences de Monastir, Département de Physique, Monastir, Tunisia

Whitney Armstrong, Sylvester Joosten, and Zein-Eddine Meziani

Argonne National Laboratory, Physics Division, Argonne, IL, USA

Thomas Hemmick

Stony Brook University, Stony Brook, NY, USA

Bernard Pire

Centre de Physique Théorique, CNRS, École polytechnique, I.P. Paris, Palaiseau, France

Pawel Sznajder and Jakub Wagner

National Centre for Nuclear Research, NCBJ, Warsaw, Poland

Johan A. Colorado-Caicedo

Centro de Investigación y de Estudios Avanzados del Instituto Politécnico Nacional, San Pedro Zacatenco, Mexico City, Mexico

Sudip Bhattachari

Idaho State University, Pocatello, ID, USA

Nikos Sparveris, Hamza Atac, Suman Shrestha, and Mazmuz. Ifat

Temple University, Philadelphia, PA, USA

Mostafa Elaasar

Southern University at New Orleans, New Orleans, LA, USA

Darko Androić

University of Zagreb, Faculty of Science, Zagreb, Croatia

Eric Fuchey

College of William & Mary, Williamsburg, Virginia, USA

Hem Bhatt

Mississippi State University, Mississippi State, MS, USA

Pawel Nadel-Turronski

University of South Carolina, Columbia, SC, USA

Xiaqing Li, Tianbo Liu, and Weizhi Xiong

Shandong University, Qingdao, Shandong, China

*: Co-spokesperson, †: Contact-spokesperson (camsonne@jlab.org)

and SoLID Collaboration

Spokesperson : Juan-Sebastian Alvarado, Alexandre Camsonne, Marie Boer,
Eric Voutier, Xinzhan Bai, Zhiwen Zhao